Hindawi
International Journal of Antennas and Propagation
Volume 2022, Article ID 3298866, 12 pages
https://doi.org/10.1155/2022/3298866

Research Article

A Compact Penta-Band Low-SAR Antenna Loaded with Split-Ring Resonator for Mobile Applications

M. Manikandan and S. Karthigai Lakshmi

Department of ECE, SSM Institute of Engineering and Technology, Dindigul, Tamil Nadu, India

Correspondence should be addressed to M. Manikandan; maniecephd2017@gmail.com

Received 12 October 2022; Revised 18 November 2022; Accepted 5 December 2022; Published 30 December 2022

Academic Editor: Ding-Bing Lin

A compact rectangular patch with dual-ring SRR (split-ring resonator) is presented in this article. An antenna is designed on FR4 substrate with an overall footprint size of 26 mm × 30 mm × 1.6 mm. The antenna presented operates in five bands from 2.95 to 3.06 GHz, 3.79 to 3.87 GHz, 4.11 to 4.19 GHz, 5.39 to 5.51 GHz, and 5.97 to 6.11 GHz. Mobile and fixed voice communication, WiMAX (Worldwide Interoperability for Microwave Access), 5G (5^{th} generation), WLAN (Wireless Local Area Network), and ISM (Industrial Scientific and Medical) are some applications that utilized the above resonating bands. The penta-band operation is due to the inclusion of dual-ring SRR. The optimum values of the critical parameter of the SRR are identified using parametric analysis, and the results are presented. The antenna is also analyzed for the SAR (specific absorption rate) values, and it was found to be less than 2 W/kg for 10 g volume of tissue. The designed antenna is fabricated and tested, and the presented results show that there is good agreement between the simulated and measured results. Penta-band operation with simple structure, stable radiation pattern, and low SAR makes this antenna more intelligent and suitable for the mobile application.

1. Introduction

The major requirement of modern wireless personal communication devices like smart phones in the past two decades is antenna, which exhibits multiband frequency of operation, omnidirectional radiation pattern, and low SAR. Bluetooth, WLAN, Satellite Communication, LTE (Long-Term Evolution), 4G (4^{th} generation), 5G (5^{th} generation), WiMAX, RFID (Radio Frequency Identification), etc. are some of the wireless standards [1] which are the essential frequency ranges needed to be incorporated in modern wireless personal communication devices like mobile phones. These devices allow only a limited space for antenna integration. This leads to another challenge for the antenna researchers to achieve the compactness of the structure. There are a variety of antenna techniques that support multiband characteristics, and the primary advantage of using the multiband antenna is that it reduces the size and complexity of the system, as a single antenna is capable of satisfying all the applications. It also eliminates the filters in the system, which results in reduced complexity, fabrication difficulty, cost, and installation requirements. The microstrip patch antenna can easily achieve such requirements [2–5] due to its low-profile characteristics.

Another essential parameter needed to be reduced in mobile device is SAR. The value of SAR in mobile phone antenna must be within the limit. According to ICNIRP (International Commission on Non-Ionizing Radiation Protection) guidelines, maximum SAR value should be 2 W/kg averaged over any 10 g volume of tissue [6], and according to the guidelines given by US FCC (Federal Communication Commission), it should be 1.6 W/kg averaged over any 1 g volume of tissue [7]. The high SAR mobile phone causes many biological effects on human body such as irreversible infertility, DNA damage, brain tumor, and so on. There are many antenna structures adopted ever since the formation of the first generation of mobile communication to reduce the SAR value. Along with main antenna structures, supplementary elements like conducting materials [8], reflector [9], ferrite shielding

[10], directional antennas [11], and resistive cards [12] are added to reduce the SAR value. Even though the above supplementary elements reduce SAR at greater level, they will improve product cost and size. The other essential parameters, such as gain, radiation efficiency was not up to the required level for above structures and also lagging in resonating with multiple frequencies. By considering these limitations, many researchers recently focused to modify the main antenna structure instead of adding supplementary elements. The AMC (artificial magnetic conductor) structure [13, 14] will reduce the SAR value and improve gain by using high impedance surface property during operating frequency. But it requires additional space and does not support multiband of operation. The SAR value can also be reduced by optimizing electric [15] and magnetic field [16]. But there is no evidence of improving gain and increasing operating bands by using this technique. The EBG (electromagnetic band gap) structure [17–19] will suppress the surface waves which will improve radiation efficiency and gain. While exhibiting stop band characteristics, it behaves like AMC structure that redirects all the radiation opposite to human head which in turn reduces the SAR value. The structure can be further optimized by reducing the size and improving return loss values. Reducing SAR without affecting antenna parameters is a challenging task.

Metamaterials are termed materials which have several distinct properties like negative permittivity and negative permeability [20–22]. These distinct properties play a major role in designing high performance antenna especially for exhibiting multiband operation [23–25] and reduce SAR at greater level [26]. The most common metamaterial structures widely used are SRRs (split-ring resonators) [27, 28] and CSRRs (complementary split-ring resonators) [29–31]. SRR may consist of two concentric split rings which act as resonators facing in opposite direction. The shape of the rings is not restricted to ring or circle structure [32], but it can also be implemented in square [33], triangular [34], and hexagonal [35] shapes. SRR acts as a resonating element due to the existence of inductor and capacitor in metal ring. The resonant frequency can be optimized by increasing the following factors such as split gap, spacing between two adjacent rings, side length, and metal width and by introducing multiple split gaps [36]. By introducing stop band at desired band of frequency, SAR can be reduced by using SRR structure. Recently, many researchers presented a SRR-inspired antenna structure that aims to achieve multiple frequency bands [37], to cut down the size [38], and to reduce SAR value [39–42] for mobile application. However, all the antennas presented in the literature have any one of the following pullbacks: unidirectional radiation pattern, extended in size, minimum number of operating bands, and high SAR, which are not suitable for modern wireless personal communication device like mobile phone.

In this paper, a penta-band simple microstrip patch antenna is presented. The antenna has a rectangular patch with dual-ring SRR as the radiating element. The antenna presented satisfies the requirement of the antenna for the mobile device. In Section 2, the evolution of the antenna is presented, in Section 3, the parametric analysis of the proposed antenna is presented, and in Section 4, the results are discussed. In Section 5, the SAR analysis is presented, followed by a conclusion.

2. Evolution and Geometry of Low-SAR Penta-Band Microstrip Patch Antenna

The proposed antenna has four design stages, starting with a simple rectangular patch antenna. The seed rectangular patch antenna is fed with a 50-ohm microstrip line. The hexagonal ring is added in the second stage, followed by another ring with the same thickness in the third stage. Finally, in the fourth stage, the split is introduced near the right side of the feed line, which converts the dual closed ring resonator into dual-ring SRR. In Figure 1, the evolution of the proposed low-SAR penta-band microstrip patch antenna is presented.

The proposed antenna is designed on a substrate with an effective dielectric constant of 4.4 and designed using CST software. The antenna is designed on a substrate with a width of 26 mm and 30 mm. First, the antenna is designed with a rectangular patch seed element presented as Ant w in Figure 1. Ant w is designed to operate from 3.09 to 4.85 GHz, and it has a frequency of resonance at 3.54 GHz. Then, the first closed ring resonator is introduced in Ant w to design Ant x. The closed ring resonator changes the current direction and shifts the operating frequency. Ant x is operating from 5.51 to 6.28 GHz. Ant y is designed by introducing another closed ring resonator of the same thickness as the first ring. The spacing between the first and second closed ring resonator is 1 mm. Further introduction of the second closed ring resonator changes the current direction, increasing the frequency of operation from 6.69 GHz to 6.91 GHz.

Finally, Ant Z is the proposed low-SAR penta-band microstrip patch antenna that is designed by cutting the part of closed rings at the right hand side of the feed line. The antenna has five resonant frequencies at 3.01 GHz, 3.83 GHz, 4.14 GHz, 5.46 GHz, and 6.06 GHz. Interpretation from the four evolution stages of the proposed structure is that the rectangular patch along with 2 hexagonal SRRs can resonate at five different frequencies. The final proposed antenna with its design parameters is depicted in Figure 2. The parameter values are presented in Table 1. The antenna is designed using the below equations. The width, length, effective permittivity, and increase in electrical length of an antenna can be calculated from equations (1)–(4), respectively.

$$W = \frac{c}{2f_r}\sqrt{\frac{2}{\varepsilon_r + 1}}, \tag{1}$$

$$L = \frac{c}{2f_r\sqrt{\varepsilon_{\text{eff}}}} - 2\Delta L, \tag{2}$$

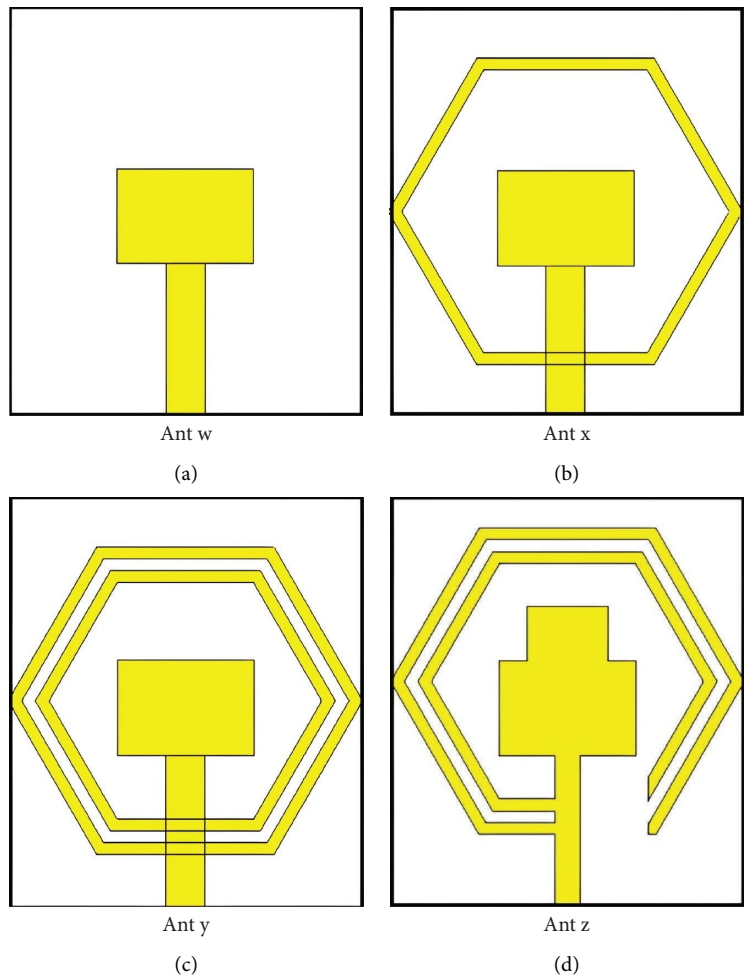

Figure 1: Evolution of the proposed low-SAR penta-band microstrip patch antenna. (a) Ant w. (b) Ant x. (c) Ant y. (d) Ant z.

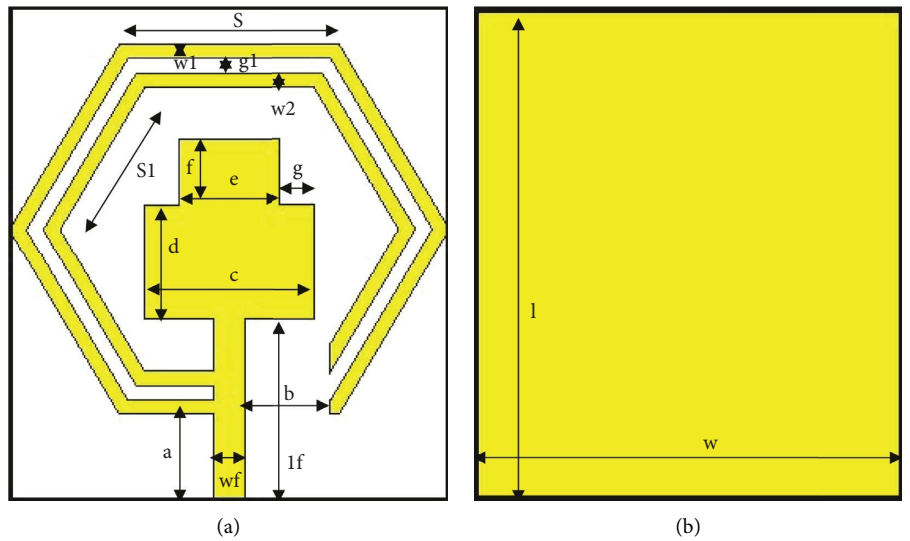

Figure 2: Final proposed low-SAR penta-band microstrip patch antenna with its design parameters. (a) Front view. (b) Back view.

Table 1: Parameter values of the proposed low-SAR penta-band microstrip patch antenna (values are in mm).

w	l	wf	lf	a	b	c	d	e
26	30	1.85	11	5.24	5	10	7	6
f	g	w_1	w_2	S	S_1	$g1$	t	h
4	2	1	1	13	10.15	1	0.0035	1.6

Table 2: Ant w vs. Ant x vs. Ant y vs. Ant z.

Antenna	Operating frequency (GHz)	Bandwidth (MHz)	Resonant frequency (GHz)	Return loss (dB)
Ant w	3.09 to 4.85	1757	3.54	−17.28
Ant x	5.51 to 6.28	773	5.81	−12.81
Ant y	6.69 to 6.91	213	6.78	−12.2
	2.95 to 3.08	95	3.01	−17.76
	3.79 to 3.87	74	3.83	−22.73
Ant z	4.11 to 4.19	79	4.14	−12.33
	5.39 to 5.51	122	5.46	−17.99
	5.97 to 6.11	149	6.04	−15.06

$$\varepsilon_{eff} = \frac{\varepsilon_r + 1}{2} + \frac{\varepsilon_r - 1}{2}\left[1 + \frac{12h}{W}\right]^{(-1/2)}, \quad (3)$$

$$\Delta L = 0.412h \frac{(\varepsilon_{\text{eff}} + 0.3)}{(\varepsilon_{\text{eff}} - 0.258)} \frac{(W/h + 0.264)}{(W/h + 0.8)}, \quad (4)$$

where c, f_r, h, and ε_{eff} are the speed of light, resonant frequency, substrate height, and effective dielectric constant, respectively.

The comparison between various antennas evolved during the design of the proposed low-SAR penta-band microstrip patch antenna is presented in Table 2. In Figure 3, the return loss of the antennas is compared and depicted. The figure shows that after introduction of SRR along with the presence of rectangular patch, the proposed structure is operating at five different bands.

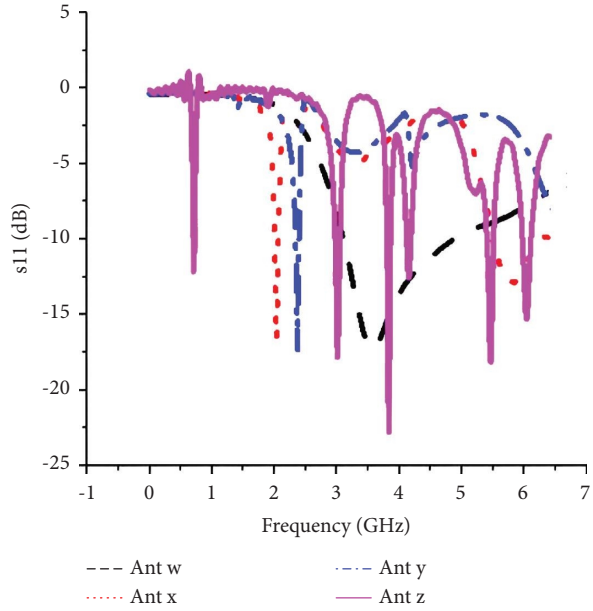

Figure 3: S_{11} comparison plot of antennas w, x, y, and z.

3. Parametric Analysis on SRR Ring

To find the optimum dimension for the critical parameters of the proposed antenna, the parametric analysis in CST is utilized. The width of the rectangular patch and ground length is analyzed parametrically but the parametric analysis of the split-ring resonator is elaborately discussed with results in this section, since it is the reason for the multiband operation of the proposed antenna. The critical parameters of the SRR, such as the width of the ring, separation between the ring, and split width in the rings, are analyzed. Then, the effect of adding the ring to the structure is also presented in this section. First, the split width is analyzed; it is increased from 3 mm to 7 mm in steps of 2 mm. The effect of increasing the split width on the return loss is presented in Figure 4. From the figure, it is observed that as the split width increases, the capacitance value increases and the frequency is shifted. For the fabrication, the optimum value of 5 mm is chosen since it achieves good impedance matching compared to 3 mm and 7 mm. Then, the width of the ring is varied from 0.5 mm to 1.5 mm in steps of 0.5 mm. The results of the same are depicted in Figure 5.

From the figure, it is observed that the width of 1 mm in both the rings can achieve good bandwidth in the resonating bands, and as a result, it is chosen for the final fabrication. Similarly, Figure 6 shows the return loss plot for various separation values between the rings. It is observed from the figure that the separation of 1 mm between the two SRR rings achieves impedance bandwidth in all the resonating bands due to distributed capacitance effect between the rings. In Figure 7, the effect of the rings on the return loss is presented. As the rings increase, the number of operating bands increases. The figure shows that the antenna is operating over a wideband of frequency without a ring. With the introduction of the first ring, the antenna is operating at four different bands. With the addition of another ring, the electrical length increases so the resonant frequency increases to five. The additional resonance is obtained because SRR rings will act as parallel LC circuits.

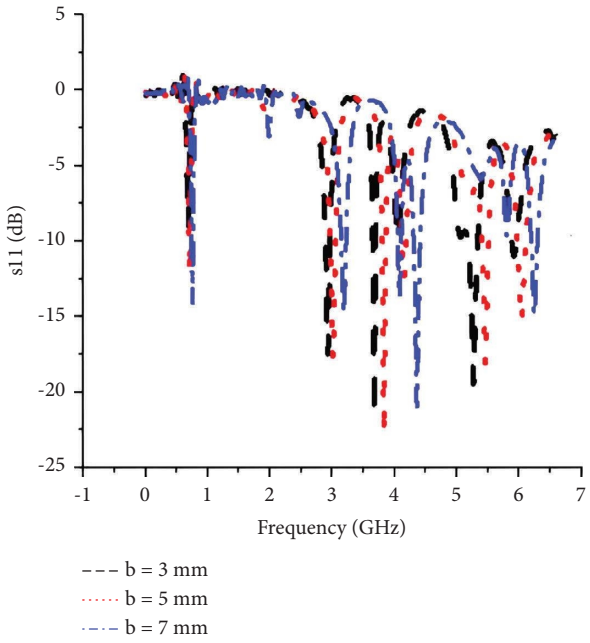

Figure 4: S_{11} comparison plot for various values of b.

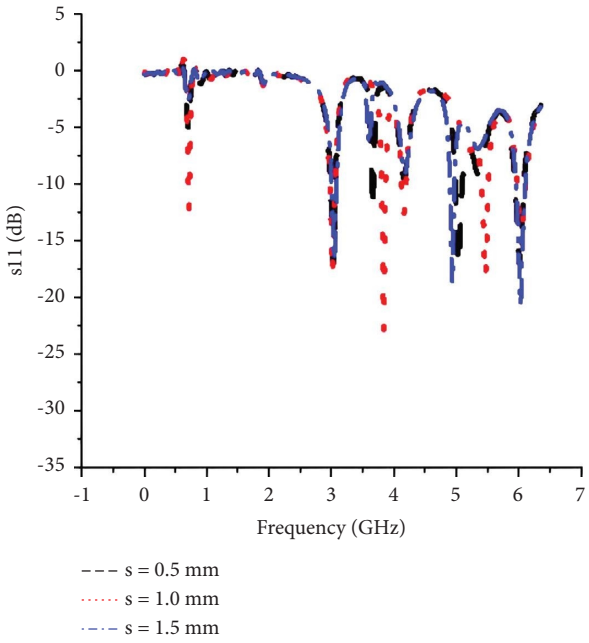

Figure 6: S_{11} comparison plot for various values of ring separation.

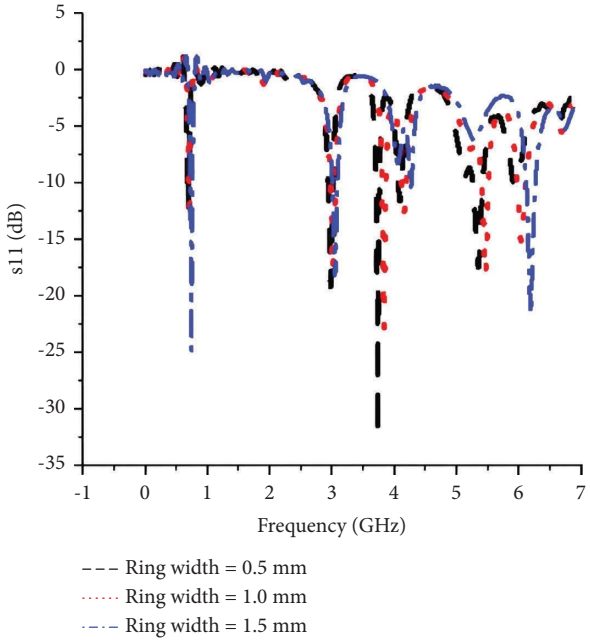

Figure 5: S_{11} comparison plot for various values of ring width.

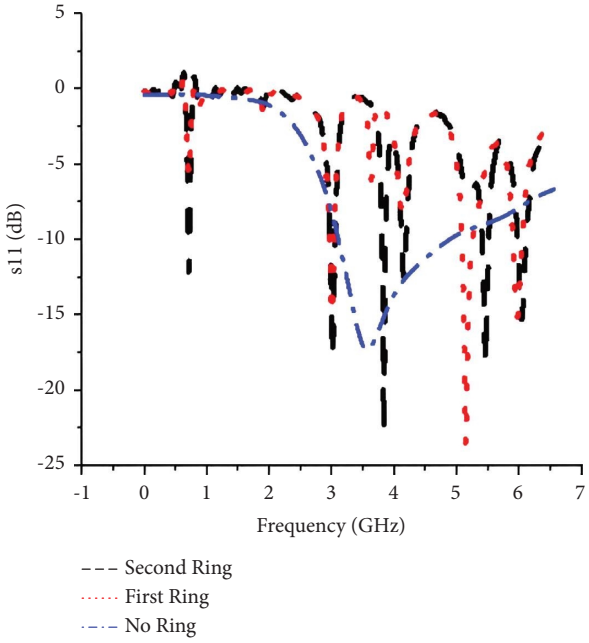

Figure 7: S_{11} comparison plot for various number of rings.

4. Result and Discussion

In Figure 8, the comparison of the return loss plot with and without a ring is presented; from the figure, it is observed that the inclusion of SRR along with rectangular patch leads to multiple resonance.

The resonant frequency of an individual hexagonal split ring has been estimated using [35]

$$f_r = \frac{1.8412 \times c}{2\pi S\sqrt{\varepsilon_r}}. \quad (5)$$

For outer hexagonal split ring having side length, $S = 13$ mm,

$$f_r = \frac{1.8412 \times 3 \times 10^8}{2 \times 3.14 \times 13 \times 10^{-3} \times \sqrt{4.4}} = 3.22 \text{ GHz}. \quad (6)$$

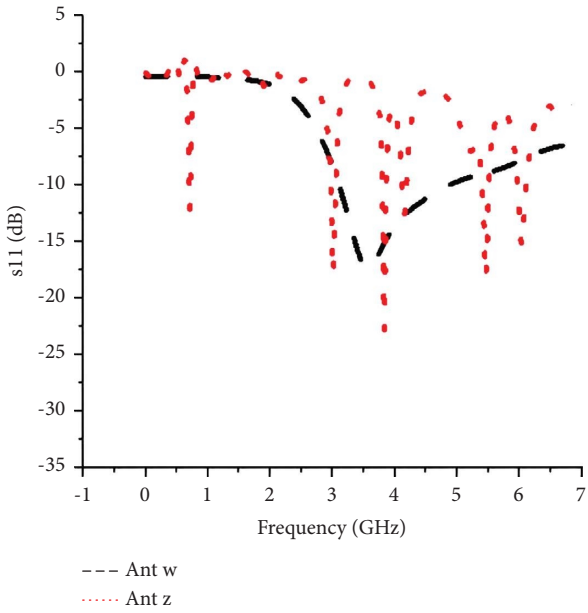

FIGURE 8: S_{11} comparison plot of the antenna with and without SRR.

For inner hexagonal split ring having side length, $S_1 = 10.15$ mm,

$$f_r = \frac{1.8412 \times 3 \times 10^8}{2 \times 3.14 \times 10.15 \times 10^{-3} \times \sqrt{4.4}} = 4.13 \text{ GHz}. \quad (7)$$

The effective dielectric constant ε_r is 4.4, from the above calculations; the side length of the hexagonal ring S determines the resonant frequency. The outer hexagonal split ring contributes 2.95 to 3.06 GHz band and inner hexagonal split ring contributes 4.11 to 4.19 GHz band. Both the resonant frequencies are shifted slightly due to coupling between two rings.

In Figure 9, the current distribution on the antenna's surface at various resonant frequencies is presented. It is clearly observed that the current is maximum at different locations for different resonating bands. In all the resonating bands, the current is highly accumulated at the dual-ring SRR, and we can conclude that the rings have the greater effect on the resonating bands. In Figure 9(e), the surface current is highly accumulated next to SRR in rectangular patch at 6.04 GHz which leads to existence of 5.97 to 6.11 GHz band. In order to get additional resonance, the two closed hexagonal rings are converted into split rings by creating a gap in right side of feed line. The gathering of charges at the edge of split gap gives rise to capacitive behavior. Therefore, the presence of inductance and capacitance makes the two hexagonal SRRs to generate two additional resonances [36]. Therefore, two split gaps result in 3.79 to 3.87 GHz and 5.39 to 5.51 GHz band, respectively. The inductance L_{SRR} and capacitance C_{SRR} of the two hexagonal SRRs are calculated [35] using (8) and (9), respectively. The resonant frequency can be determined from (10), where $l = 13$ mm and 10.15 mm for outer and inner hexagonal SRR's side length, respectively, $N = 2$ which is the number of hexagonal SRR, $w = 1$ mm which is the width of both hexagonal SRRs, $s = 1$ mm which is the distance between two SRRs, and $K(k)$ is the first kind of elliptical integral identity.

$$L_{\text{SRR}} = 4 * \mu_0 * [l - (N-1)(w+s)] * \left[\ln\left(\frac{0.98 * [l - (N-1)(w+s)]}{(N-1)(w+s)}\right) + \left(\frac{1.84 * [l - (N-1)(w+s)]}{(N-1)(w+s)}\right)\right], \quad (8)$$

$$C_{\text{SRR}} = \frac{N-1}{2} * [2l - (2N-1)(w+s)] * \varepsilon_0 * \left(\frac{K\left(\sqrt{1-k^2}\right)}{K(k)}\right), \quad (9)$$

where $k = (s/2w + s)$.

$$F = \frac{1}{2\Pi\sqrt{L_{\text{SRR}} * C_{\text{SRR}}}}. \quad (10)$$

In Figure 10, the radiation pattern of the proposed low-SAR penta-band antenna is presented; it is observed from the figure that the pattern is stable in both E and H planes. The E plane exhibits a dumbbell-shaped pattern while the H plane exhibits the omnidirectional pattern, which is the need for the personal wireless communication standard application. A perfect dumbbell-shaped pattern and omnidirectional pattern was achieved in both E plane and H plane, respectively, for 4.14 GHz. In Figure 11, the fabricated antenna is presented. The comparison between the simulated and measured results of S_{11} is presented in Figure 12. In Figure 13, the simulated and measured gain was presented concerning the operating frequency.

The proposed antenna exhibits gain above 2 dBi in all the resonating bands, and the maximum gain of the proposed antenna is 6.2 dBi.

5. SAR Analyses

We used three layers of bespoke body tissue in this study. The model is made up of a 10 mm thick muscle layer, a 6 mm thick fat layer, and a 0.5 mm thick skin layer. The personalized body tissue was used to assess the SAR, which defines the amount of energy absorbed by body tissues, and explore the influence of

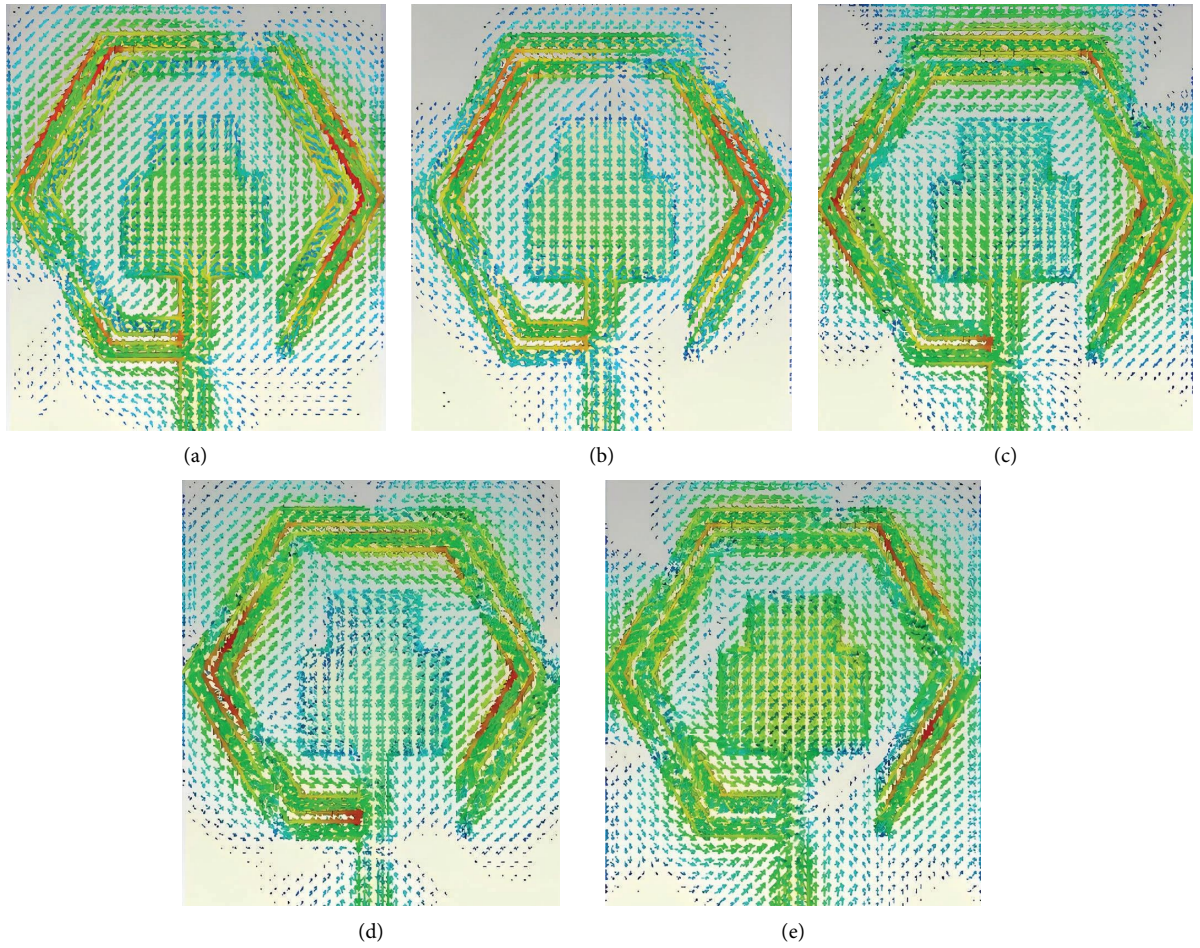

Figure 9: Distribution of surface current on the proposed low-SAR penta-band microstrip patch antenna. (a) 3.01 GHz. (b) 3.83 GHz. (c) 4.14 GHz. (d) 5.46 GHz. (e) 6.04 GHz.

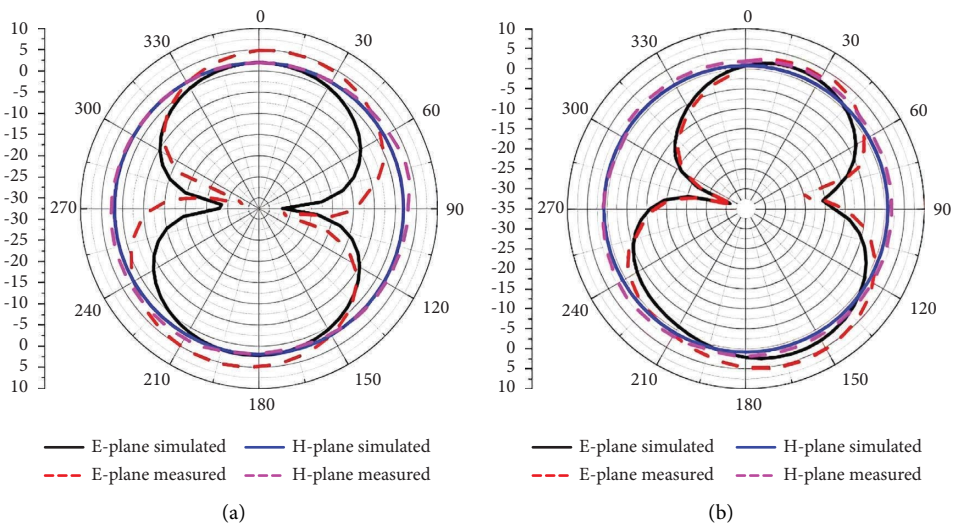

Figure 10: Continued.

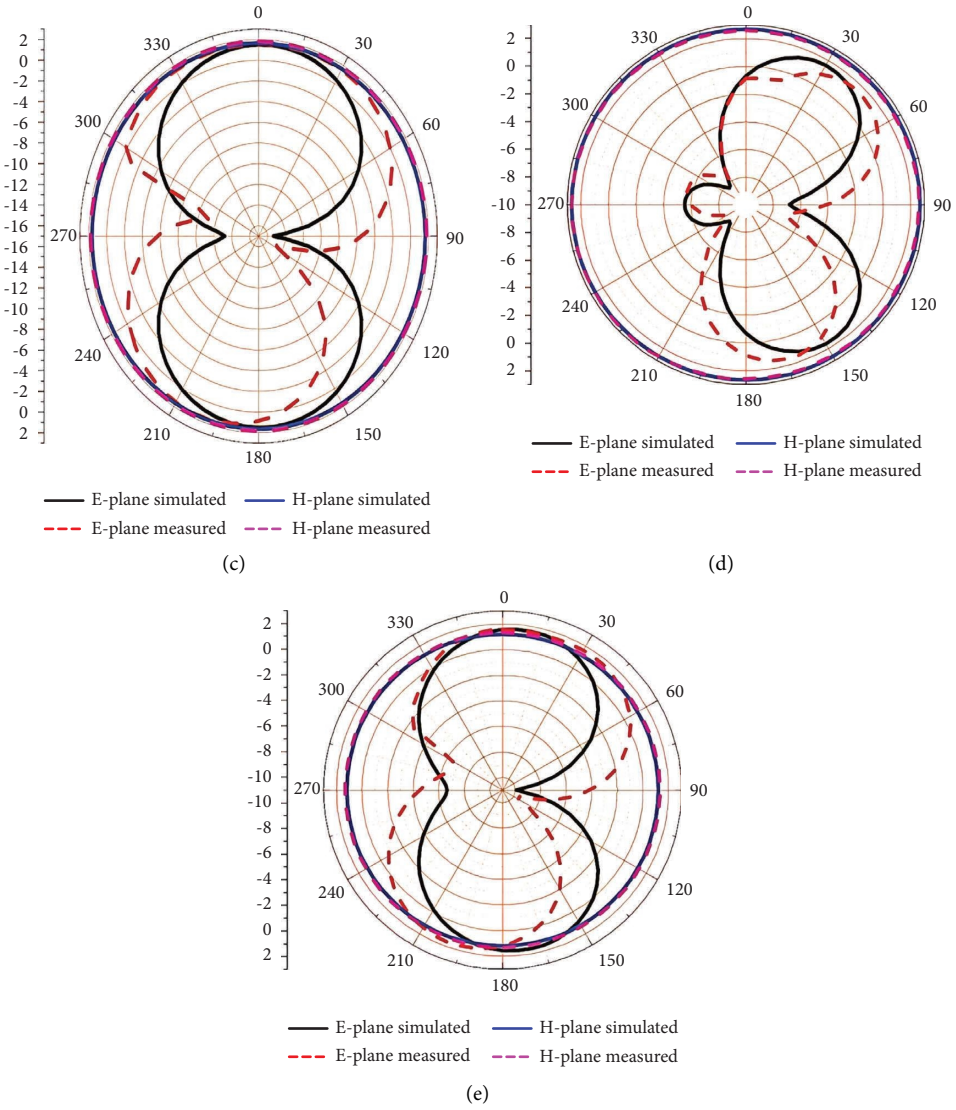

Figure 10: *E* plane and *H* plane of the proposed low-SAR penta-band microstrip patch antenna. (a) 3.01 GHz. (b) 3.83 GHz. (c) 4.14 GHz. (d) 5.46 GHz. (e) 6.04 GHz.

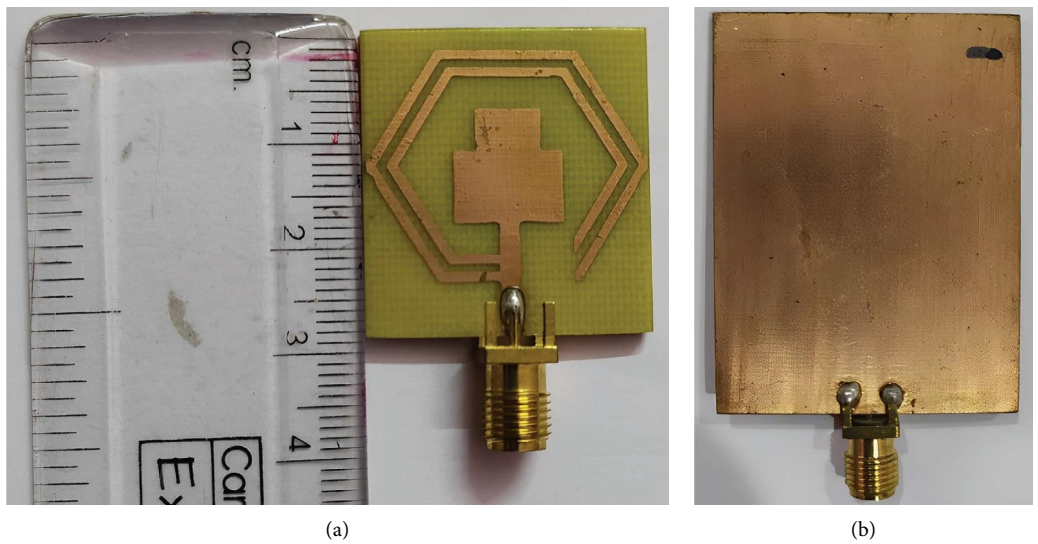

Figure 11: Front view and back view of fabricated antenna. (a) Front view. (b) Back view.

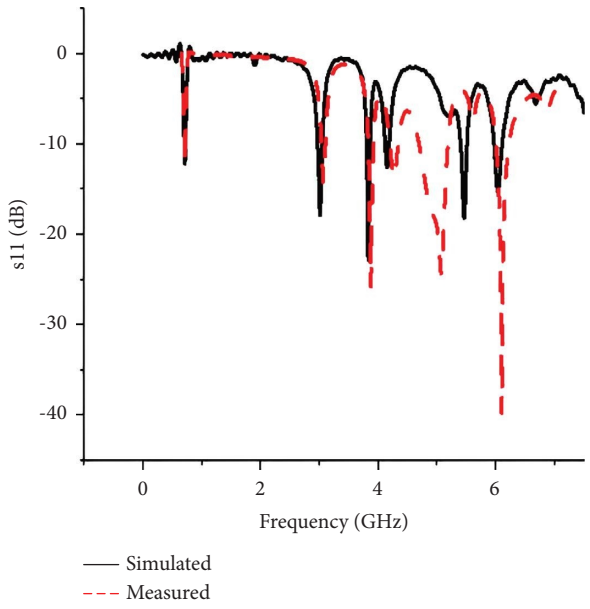

Figure 12: Simulated vs. measured results of S_{11}.

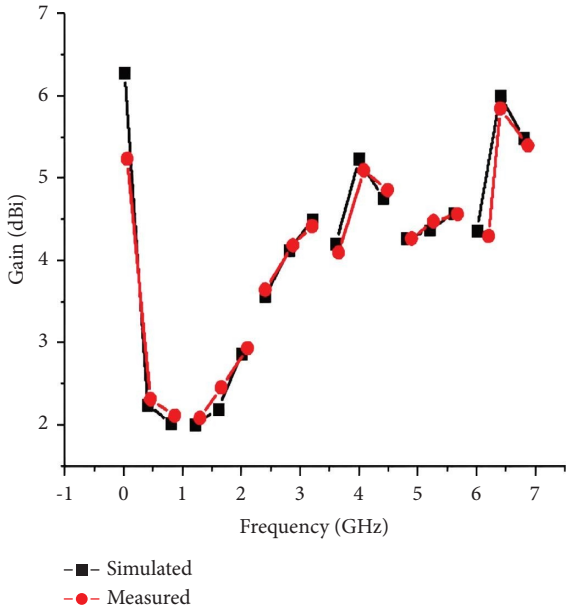

Figure 13: Simulated vs. measured results of gain.

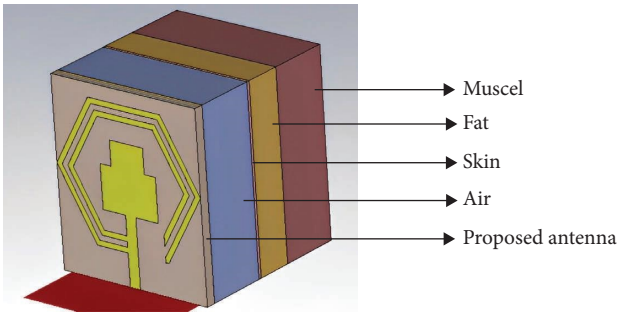

Figure 14: Proposed low-SAR penta-band microstrip patch antenna with human model.

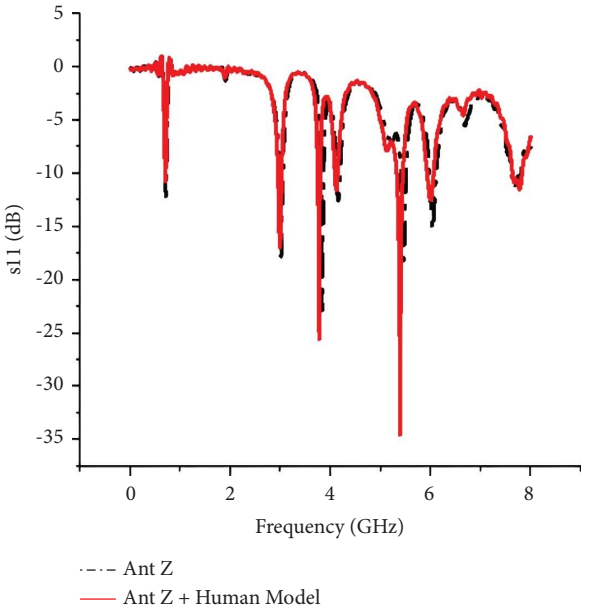

Figure 15: S_{11} comparison of the proposed antenna with and without human model.

the human body on wearable antenna performance. Because the human body is a frequency-dispersive material, the higher frequency bands will be influenced more when the antenna touches the skin. On the other hand, adding spacing will enhance impedance bandwidth and impedance matching.

In Figure 14, the proposed antenna with the fragmented human phantom model in the CST environment is presented. In Figure 15, the effect of the human body in the return loss and frequency of operation is presented. Due to the robustness of the antenna, the centre frequency of the supported applications was not detuned. There was a good agreement between the results, as shown in Figure 15. Because the human body is a complex medium with high permittivity, placing the antenna closer to the body's tissues significantly reduced the gain and efficiency of the antenna. IEEE/IEC 62704-1 averaged on 10 g was used to calculate the SAR value of the biological tissues. Mathematically, SAR is calculated by $\sigma\,[|E|^2/\rho]$, where σ is the tissue conductivity, E is the electric field, and ρ is the mass density of the tissue. The maximum limit of SAR for 10 g volume of tissue is 2 W/kg. In Figure 16, the simulated SAR is presented, from which at all the resonant frequencies, the proposed structure exhibits SAR < 2 W/kg. So, the proposed antenna could be used in personal communication devices. In Table 3, the numerical values of the SAR are presented against the resonating frequencies.

In Table 4, the proposed antenna is compared with literature antennas presented for mobile applications. The recent methodologies adopted to reduce SAR value in mobile phone antenna were taken for comparing proposed antenna. From the comparison, the AMC structure reduces the SAR value with better gain, but the number of operating bands is very limited; additional AMC structure is developed along with main structure. By optimizing electric and magnetic fields, SAR can be reduced, but there is no evidence of gain improvement

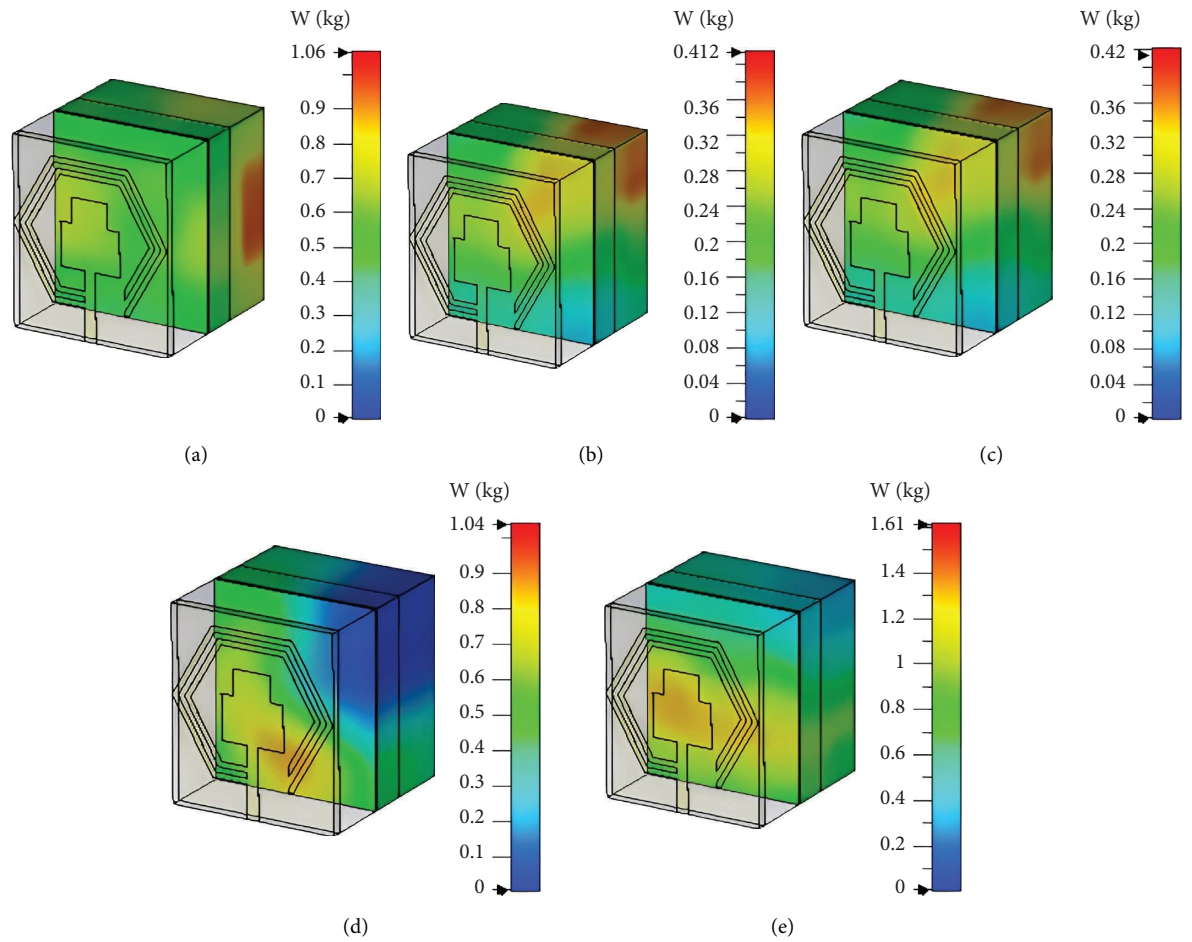

Figure 16: SAR analysis at various resonating frequencies. (a) 3.01 GHz. (b) 3.83 GHz. (c) 4.14 GHz. (d) 5.46 GHz. (e) 6.04 GHz.

Table 3: Centre frequency vs. SAR.

Centre frequency (GHz)	3.01	3.83	4.14	5.46	6.04
SAR (W/kg)	1.06	0.412	0.42	1.04	1.61

Table 4: Proposed antenna vs. literature antennas.

Ref no. and year	Applied design methods	Dimension (mm^2)	Requirement and name of additional structure	No. of operating bands	Maximum bandwidth	Minimum return loss (dB)	Maximum gain (dBi)	Minimum SAR value
Reference [13], 2021	AMC structure	40.5×40.5	Yes and AMC structure	1	510 MHz	−40	7.47	4.8 (1 gram)
Reference [14], 2020	AMC structure	30.54×30.54	Yes and AMC structure	1	472 MHz	−16	8.69	0.353 (10 gram)
Reference [15], 2021	Optimizing *E* field	154×74	Yes and metal rim	4	980 MHz	−27	Not specified	1.19 (10 gram)
Reference [16], 2021	Optimizing *H* field	151×71	Yes and metallic bezels	1	90 MHz	−24	Not specified	0.183 (10 gram)
Reference [17], 2022	EBG structure	50.3×40	No	3	1 GHz	Poor	2.5	0.27 (1 gram)
Reference [18], 2019	EBG structure	91×91	No	1	244 MHz	−24	2.95	0.498 (1 gram)
Reference [19], 2021	EBG structure	36.67×40	Yes and dual feeding	4	750 MHz	−40	4.55	0.62 (10 gram)
Reference [40], 2021	SRR structure	20×13	Yes and SRR structure	3	1.9 GHz	−34	3	1.64 (1 gram)
Reference [41], 2021	SRR structure	14×28	No	4	550 MHz	−24	Not specified	0.21 (1 gram)
Reference [42], 2021	SRR structure	90×42	Yes and SRR structure	2	60 MHz	−38	Not specified	0.50 (10 gram)
Proposed antenna	SRR structure	30×26	No additional structure	5	400 MHz	−35	6.2	0.41 (10 gram)

using those structures. Even though EBG structures reduce SAR at greater level without adding additional structures with more resonant frequencies, gain is lower than that of other methodologies. The SRR available in the literature reduces SAR either by adding additional structures or by compromising gain values. But the proposed compact rectangular patch antenna loaded with split-ring resonator reduces SAR at a greater level in all five different resonant frequencies with improved gain and minimum return loss.

6. Conclusions

A simple compact rectangular patch antenna with dual-ring SRR is presented for the modern wireless personal communication. The antenna is designed and fabricated on an FR4 substrate. The proposed structure operates on five different bands with resonance at 3.0 GHz, 3.8 GHz, 4.1 GHz, 5.4 GHz, and 6.0 GHz. In all the operating bands, the impedance bandwidth is well maintained with maximum gain of 6.2 dBi. The introduction of the SRR is responsible for the multiband operation, which is evident from the parameter analysis and surface current distribution presented in this article. The critical antenna parameters are analyzed, and its optimum values are identified using parametric analysis. The antenna is further analyzed for the SAR level, and it is found that the antenna exhibits very low values of SAR at all the five resonating frequencies. The simulated SAR value at all the resonating bands is less than 2 W/kg. The depicted simulated results of S_{11} and radiation pattern are on par with the measured results. The antenna is further validated with the surface current, gain, *E* Plane, and *H* plane pattern results. Simple structure with stable pattern, reasonable gain, good impedance bandwidth, and low SAR makes the proposed antenna more suitable for the 5G mobile application.

Data Availability

The data used to support the findings of this study are included within the article.

Disclosure

This study was performed as a part of the employment of the authors.

Conflicts of Interest

The authors declare that they have no conflicts of interest.

References

[1] R. Saleem, M. Bilal, H. T. Chattha, S. Ur Rehman, A. Mushtaq, and M. F. Shafique, "An FSS based multiband MIMO system incorporating 3D antennas for WLAN/WiMAX/5G cellular and 5G wi-fi applications," *IEEE Access*, vol. 7, pp. 144732–144740, 2019.

[2] K. Sultan, M. Ikram, and N. Nguyen-Trong, "A multiband multi beam antenna for sub-6 GHz and mm-wave 5G applications," *IEEE Antennas and Wireless Propagation Letters*, vol. 21, no. 6, pp. 1278–1282, June 2022.

[3] H. Li, J. Du, X.-X. Yang, and S. Gao, "Low-profile all-textile multiband microstrip circular patch antenna for WBAN applications," *IEEE Antennas and Wireless Propagation Letters*, vol. 21, no. 4, pp. 779–783, April 2022.

[4] Y. Liu, Y. Li, L. Ge, J. Wang, and B. Ai, "A compact hepta-band mode-composite antenna for sub (6, 28, and 38) GHz applications," *IEEE Transactions on Antennas and Propagation*, vol. 68, no. 4, pp. 2593–2602, April 2020.

[5] A. Abdalrazik, A. Gomaa, and A. A. Kishk, "A hexaband quad-circular-polarization slotted patch antenna for 5G, GPS, WLAN, LTE, and radio navigation applications," *IEEE Antennas and Wireless Propagation Letters*, vol. 20, no. 8, pp. 1438–1442, 2021.

[6] International Commission on Non-Ionizing Radiation Protection, "Health issues related to the use of hand-held radiotelephones and base transmitters," *Health Physics*, vol. 70, no. 4, pp. 587–593, 1996.

[7] IEEE, "IEEE standard for safety levels with respect to human exposure to radio frequency electromagnetic fields, 3 kHz to 300 GHz," *IEEE Std C95*, pp. 1–238, 2006.

[8] M. Faruque, M. Islam, and N. Misran, "Analysis of SAR levels in human head tissues for four types of antennas with portable telephones," *Australian Journal of Basic and Applied Sciences*, vol. 5, pp. 96–107, 2011.

[9] M. Haridim, "Use of rod reflectors for SAR reduction in human head," *IEEE Transactions on Electromagnetic Compatibility*, vol. 58, no. 1, pp. 40–46, 2016.

[10] M. T. Islam, M. R. I. Faruque, and N. Misran, "Design analysis of ferrite sheet attachment for SAR reduction in human head," *Progress In Electromagnetics Research*, vol. 98, pp. 191–205, 2009.

[11] K. W. Kim and Y. Rahmat-Samii, "Handset antennas and humans at Ka-band: the importance of directional antennas," *IEEE Transactions on Antennas and Propagation*, vol. 46, no. 6, pp. 949-950, 1998.

[12] H.-H. Chou, H. T. Hsu, H. T. Chou, K. H. Liu, and F. Y. Kuo, "reduction of peak SAR in human head for handset applications with resistive sheets (R-Cards)," *Progress In Electromagnetics Research*, vol. 94, pp. 281–296, 2009.

[13] P. Saha, D. Mitra, and S. K. Parui, "Control of gain and SAR for wearable antenna using AMC structure," *Radio Engineering*, vol. 30, no. 1, pp. 81–88, 2021.

[14] A. R. O. Mumin, R. Alias, J. Abdullah, S. H. Dahlan, J. Ali, and S. K. Debnath, "Design a compact square ring patch antenna with AMC for SAR reduction in WBAN applications," *Bulletin of Electrical Engineering and Informatics*, vol. 9, no. 1, pp. 370–378, 2020.

[15] H. H. Zhang, G. G. Yu, Y. Liu, Y. X. Fang, G. Shi, and S. Wang, "Design of low-SAR mobile phone antenna: theory and applications," *IEEE Transactions on Antennas and Propagation*, vol. 69, no. 2, pp. 698–707, 2021.

[16] B. Lu, B. Pang, W. Hu, and W. Jiang, "Low-SAR antenna design and implementation for mobile phone applications," *IEEE Access*, vol. 9, pp. 96444–96452, 2021.

[17] M. M. Munde, A. B. Nandgaonkar, and S. B. Deosarkar, "Ultra-wideband circular microstrip antenna with hybrid EBG for reduced SAR," *Advanced Electromagnetics*, vol. 11, no. 1, pp. 51–57, 2022.

[18] M. Munde, A. Nandgaonkar, and S. Deosarkar, "Low specific absorption rate antenna using electromagnetic band gap structure for long Term evolution band 3 application," *Progress In Electromagnetics Research M*, vol. 80, pp. 23–34, 2019.

[19] M. Munde, A. Nandgaonkar, and S. Deosarkar, "Performance optimization of dual-feed UWB annular ring antenna with circular DGS and EBG for SAR reduction," *Progress In Electromagnetics Research C*, vol. 115, pp. 51–64, 2021.

[20] C. Milias, R. B. Andersen, P. I. Lazaridis et al., "Metamaterial-inspired antennas: a review of the state of the art and future design challenges," *IEEE Access*, vol. 9, pp. 89846–89865, 2021.

[21] N. Suresh Kumar, K. C. B. Naidu, P. Banerjee, T. Anil Babu, and B. Venkata Shiva Reddy, "A review on metamaterials for device applications," *Crystals*, vol. 11, no. 5, p. 518, 2021.

[22] X. Wu, X. Wen, J. Yang, S. Yang, and J. Xu, "Metamaterial structure based dual-band antenna for WLAN," *IEEE Photonics Journal*, vol. 14, no. 2, pp. 1–5, 2022.

[23] M. M. Hasan, M. R. I. Faruque, and M. T. Islam, "Dual band metamaterial antenna for LTE/Bluetooth/WiMAX system," *Scientific Reports*, vol. 8, no. 1, p. 1240, 2018.

[24] D. Gallardo, D. Monasterio, R. Finger, F. P. Mena, and L. Bronfman, "A compact metamaterial-based antenna for multiband phased array applications," *IEEE Transactions on Antennas and Propagation*, vol. 69, no. 12, pp. 8872–8877, 2021.

[25] R. K. Saraswat, "A hybrid fractal metamaterial inspired multiband antenna for wireless applications," *Wireless Personal Communications*, vol. 124, no. 3, pp. 2593–2612, 2022.

[26] T. Ramachandran, M. R. I. Faruque, E. Ahamed, and S. Abdullah, "Specific absorption rate reduction of multi split square ring metamaterial for L-and S-band application," *Results in Physics*, vol. 15, Article ID 102668, 2019.

[27] S. Liu, Z. Wang, and Y. Dong, "Compact wideband SRR-inspired antennas for 5G microcell applications," *IEEE Transactions on Antennas and Propagation*, vol. 69, no. 9, pp. 5998–6003, 2021.

[28] V. Rajesh kumar and R. Rajkumar, "SRR loaded compact triband MIMO antenna for WLAN/WiMAX applications," *Progress In Electromagnetics Research Letters*, vol. 95, pp. 43–53, 2021.

[29] R. Hou, J. Ren, M. Zuo, X. Du, and Y. Z. Yin, "Magneto electric dipole filtering antenna based on CSRR with third harmonic suppression," *IEEE Antennas and Wireless Propagation Letters*, vol. 20, no. 7, pp. 1337–1341, 2021.

[30] A. El Yousfi, A. Lamkaddem, K. A. Abdalmalak, and D. Segovia-Vargas, "A miniaturized triple-band and dual-polarized monopole antenna based on a CSRR perturbed ground plane," *IEEE Access*, vol. 9, pp. 164292–164299, 2021.

[31] S. Prasad Jones Christydass and N. Gunavathi, "Dual-band complementary split-ring resonator engraved rectangular monopole for GSM and WLAN/WiMAX/5G sub-6 GHz band (new radio band)," *Progress In Electromagnetics Research C*, vol. 113, pp. 251–263, 2021.

[32] P. K. Sharma and N. Gupta, "A CPW-fed circular SRR-inspired flexible antenna using polydimethylsiloxane (PDMS) substrate for WLAN and WBAN applications," *IEEE Journal on Flexible Electronics*, vol. 1, no. 1, pp. 39–46, 2022.

[33] M. R. I. Faruque, M. T. Islam, and M. A. M. Ali, "A new design of metamaterials for SAR reduction," *Measurement Science Review*, vol. 13, no. 2, pp. 70–74, 2013.

[34] M. R. I. Faruque and M. T. Islam, "Novel triangular metamaterial design for electromagnetic absorption reduction in human head," *Progress In Electromagnetics Research*, vol. 141, pp. 463–478, 2013.

[35] R. Samson Daniel and R. Selvaraj, "A low-profile spilt ring monopole antenna loaded with hexagonal split ring resonator for RFID applications," *Progress In Electromagnetics Research M*, vol. 92, pp. 169–179, 2020.

[36] P. Kumar, T. Ali, and M. M. M. Pai, "Electromagnetic metamaterials: a new paradigm of antenna design," *IEEE Access*, vol. 9, pp. 18722–18751, 2021.

[37] N. ThamilSelvi, P. Thiruvalar Selvan, S. P. K. Babu, and R. Pandeeswari, "Multiband metamaterial-inspired antenna using split ring resonator," *Computers & Electrical Engineering*, vol. 84, Article ID 106613, 2020.

[38] A. M. Tamim, M. R. I. Faruque, and M. T. Islam, "Metamaterial-inspired electrically small antenna for microwave applications," *Proceedings of the Institution of Mechanical Engineers, Part L: Journal of Materials: Design and Applications*, vol. 236, no. 11, pp. 2230–2241, 2021.

[39] A. M. Tamim, M. R. I. Faruque, E. Ahamed, and M. T. Islam, "Electromagnetic absorption of SRR based double-inverse E-shaped metamaterial for DCS, EESC, 5G, and WiMAX applications," *Chinese Journal of Physics*, vol. 66, pp. 349–361, 2020.

[40] S. Imaculate Rosaline, "A triple-band antenna with a metamaterial slab for gain enhancement and specific absorption rate (SAR) reduction," *Progress In Electromagnetics Research C*, vol. 109, pp. 275–287, 2021.

[41] T. Ramachandran, M. R. I. Faruque, A. M. Siddiky, and M. T. Islam, "Reduction of 5G cellular network radiation in wireless mobile phone using an asymmetric square shaped passive metamaterial design," *Scientific Reports*, vol. 11, no. 1, p. 2619, 2021.

[42] A. M. Tamim, M. R. I. Faruque, M. U. Khandaker, M. T. Islam, and D. A. Bradley, "Electromagnetic radiation reduction using novel metamaterial for cellular applications," *Radiation Physics and Chemistry*, vol. 178, Article ID 108976, 2021.